

Robust autofocusing propagation in turbulence

Na-Na Liu(刘娜娜), Liu Tan(谭柳), Kai-Jian Chen(陈凯健),Pei-Long Hong(洪佩龙), Xiao-Ming Mo(莫小明), Bing-Suo Zou(邹炳锁), Yu-Xuan Ren(任煜轩), and Yi Liang(梁毅)

Citation: Chin. Phys. B, 2024, 33 (**6**): 064201. DOI: 10.1088/1674-1056/ad2bf4
Journal homepage: http://cpb.iphy.ac.cn; http://iopscience.iop.org/cpb

What follows is a list of articles you may be interested in

A global model of intensity autocorrelation to determine laser pulse duration

Yufei Peng(彭雨菲), Liqiang Liu(刘励强), Lihong Hong(洪丽红), and Zhiyuan Li(李志远)
Chin. Phys. B, 2024, 33 (**5**): 054207. DOI: 10.1088/1674-1056/ad1c57

Optical trapping capability of tornado circular Pearcey beams

Na-Na Liu(刘娜娜), Xiao-Ying Tang(唐晓莹), Shun-Yu Liu(刘舜禹), and Yi Liang(梁毅)
Chin. Phys. B, 2024, 33 (**5**): 054201. DOI: 10.1088/1674-1056/ad3347

Singular optical propagation properties of two types of one-dimensional anti-*PT*-symmetric periodic ring optical waveguide networks

Yanglong Fan(樊阳龙), Xiangbo Yang(杨湘波), Huada Lian(练华达), Runkai Chen(陈润楷),Pengbo Zhu(朱蓬勃), Dongmei Deng(邓冬梅), Hongzhan Liu(刘宏展), and Zhongchao Wei(韦中超)
Chin. Phys. B, 2024, 33 (**3**): 034201. DOI: 10.1088/1674-1056/ad12ab

Bessel—Gaussian beam-based orbital angular momentum holography

Jiaying Ji(季佳滢), Zhigang Zheng(郑志刚), Jialong Zhu(朱家龙), Le Wang(王乐), Xinguang Wang(王新光), and Shengmei Zhao(赵生妹)
Chin. Phys. B, 2024, 33 (**1**): 014204. DOI: 10.1088/1674-1056/acfdff

Theoretical research on the transverse spin of structured optical fields inside a waveguide

Zhiyong Wang(王智勇), Xiangru Wang(汪相如), Anran Li(李岸然), Kaiqiang Zhang(张开强), Yukun Ji(纪玉坤), and Mingyu Zhong(钟明玉)
Chin. Phys. B, 2023, 32 (**6**): 064207. DOI: 10.1088/1674-1056/acbf28

Robust autofocusing propagation in turbulence

Na-Na Liu(刘娜娜)[1], Liu Tan(谭柳)[1], Kai-Jian Chen(陈凯健)[1], Pei-Long Hong(洪佩龙)[2], Xiao-Ming Mo(莫小明)[1], Bing-Suo Zou(邹炳锁)[1], Yu-Xuan Ren(任煜轩)[3], and Yi Liang(梁毅)[1,†]

[1] *Guangxi Key Laboratory for Relativistic Astrophysics, Center on Nanoenergy Research, School of Physical Science and Technology, Guangxi University, Nanning* 530004, *China*
[2] *School of Mathematics and Physics, Anqing Normal University, Anqing* 246133, *China*
[3] *Institute for Translational Brain Research, MOE Frontiers Center for Brain Science, Fudan University, Shanghai* 200032, *China*

(Received 22 December 2023; revised manuscript received 5 February 2024; accepted manuscript online 22 February 2024)

Turbulence in complex environments such as the atmosphere and biological media has always been a great challenge to the application of beam propagation in optical communication, optical trapping and manipulation. To overcome this challenge, this study comprehensively investigates the robust propagation of traditional Gaussian and autofocusing beams in turbulent environments. In order to select stable beams that exhibit high intensity and high field gradient at the focal position in complex environments, Kolmogorov turbulence theory is used to simulate the propagation of beams in atmospheric turbulence based on the multi-phase screen method. We systematically analyze the intensity fluctuations, the variation of the coherence factor and the change in the scintillation index with propagation distance. The analysis reveals that the intensity fluctuations of autofocusing beams are significantly smaller than those of Gaussian beams, and the coherence of autofocusing beams is better than that of Gaussian beams under turbulence. Moreover, autofocusing beams exhibit less oscillation than Gaussian beams, indicating that autofocusing beams propagate in complex environments with less distortion and intensity fluctuation. Overall, this work clearly demonstrates that autofocusing beams exhibit higher stability in propagation compared with Gaussian beams, showing great promise for applications such as optical trapping and manipulation in complex environments.

Keywords: propagation, beams, autofocusing, turbulence

PACS: 42.25.Bs, 42.25.Dd, 42.68.Ay, 42.25.Fx **DOI:** 10.1088/1674-1056/ad2bf4

1. Introduction

Due to strong absorption and scattering, turbulence in complex environments such as the atmosphere[1,2] and complex biological media[3] has been a major obstacle to beam propagation in optical communication,[4] optical trapping and manipulation.[3,5] Various methods have been developed to overcome this challenge. For example, the use of structured light including Bessel–Gaussian, Hermite–Gaussian, Laguerre–Gaussian, vortex beams and vector beams, has effectively mitigated the effects of turbulence on optical systems.[1,2] While most current research on structured light in turbulence has been focused on optical communication, structured light is also promising in optical trapping and manipulation.[5] This is especially true when optical tweezers work in complex environments where scattering and turbulence pose challenges to optical trapping and manipulation.[3]

As we know, excellent focusing of a beam is critical for achieving good optical trapping and manipulation in complex environments. At present, a popular method is to reshape the wavefront and achieve beam focusing through random media.[6–10] However, the recovery of the optimum wavefront requires careful and complicated pre-compensation for beam scattering. Thus, alternative routes are still in high demand. Recently, autofocusing beams[11,12] have gained popularity with optical tweezers and manipulation.[3,5,13–18] Without traditional lenses or nonlinearity, autofocusing beams allow sudden autofocusing, giving rise to enhanced intensity at the focus. Previous works have demonstrated that Gaussian beams are susceptible to severe distortions and continuous "center of mass" hopping under turbulence, while Airy beams experience significantly less distortion and drift.[19,20] Moreover, when a Gaussian beam passes through a scattering medium, random speckles form due to light scattering[21] whereas Airy beams maintain their basic characteristics, except for a reduction in intensity due to scattering. By using rotational symmetry, a traditional Airy beam can be extrapolated to a circular Airy beam (CAB); CABs suggest an autofocusing feature and may have greater robustness during propagation in complex environments.

In contrast to CABs, a circular Pearcey beam (CPB), which is derived from another kind of accelerating beam called a Pearcey beam,[22,23] offers better autofocusing performance. CPB has a shorter autofocusing distance and stronger peak focusing intensity and eliminates post-focus oscillations, making it more effective for optical manipulation. Moreover, circular Pearcey vortex beam in complex environments can, in theory, propagate better than circular Airy vortex beam,[24] implying that CPB may also have better performance than CAB. There-

†Corresponding author. E-mail: liangyi@gxu.edu.cn

© 2024 Chinese Physical Society and IOP Publishing Ltd

fore, to confirm the potential of CABs and CPBs in optical manipulation under complex environments, we theoretically and experimentally investigate how the autofocusing propagation of CABs and CPBs changes with the degree of air turbulence. Moreover, we also compare CABs and CPBs with equivalent Gaussian beams selected according to two different criteria: the same focal spot-size Gaussian beam (SSGB) and the same envelope Gaussian beam (SEGB). The SEGB beam width equals the diameters of the main rings of the CAB and CPB.[17,25] We analyze the distortion and intensity fluctuation of these beams passing through complex environments and compare their robustness in focusing propagation. Our results show that autofocusing beams can resist air turbulence and light scattering, implying potential robustness in penetrating tissues for excellent optical trapping and manipulation. Furthermore, our findings indicate that CPB performs better than an SSGB, SEGB or CAB in turbulence. Overall, our study highlights the potential of autofocusing beams as a superior option for applications that require robustness in complex environments.

2. Theory and experiment

The input fields of the Gaussian beam, CAB and CPB are respectively expressed as[23,26]

$$\psi_{\mathrm{GB}}(r,0)=A_0\exp\left(-\frac{r^2}{w_0^2}\right), \tag{1}$$

$$\psi_{\mathrm{CAB}}(r,0)=A_1\mathrm{Ai}\left[\frac{c_1-r}{w_1}\right]\exp\left[\frac{\alpha(c_1-r)}{w_1}\right]q(r), \tag{2}$$

$$\psi_{\mathrm{CPB}}(r,0)=A_2\mathrm{Pe}\left[\frac{(c_2-r)}{w_2},0\right]q(r), \tag{3}$$

where A_0, A_1, A_2 are the amplitudes, $\mathrm{Ai}(x)=\int_0^\infty\cos\left(\frac{t^3}{3}+xt\right)\mathrm{d}t/\pi$ is the Airy function, $\mathrm{Pe}(u,v)=\int_{-\infty}^{\infty}\exp\left[\mathrm{i}\left(t^4+t^2u+tv\right)\right]\mathrm{d}t$ is the Pearcey function, $r=\sqrt{x^2+y^2}$ is the radial coordinate, w_0 is the waist radius of the Gaussian beam, c_1, c_2 are parameters controlling the initial radii of the CAB and CPB, w_1, w_2 are the transverse scale factors and α is the exponential decay factor. $q(r)=\mathrm{rect}(r/r_1)$ $(r\geq 0)$ is an indicator used to limit the power for generating the beams in experiment and r_1 is used to restrict the beam range. To compare the propagation behavior effectively and consistently, we adopted appropriate parameters to give beams the same focal length and spot size or initial envelope (see supplementary Section 1 for details). In addition, $\lambda=532$ nm and input power $P=1$ W.

In the experiments, SSGB and SEGB are focused by an additional lens (L3 in Fig. 1(a1) with a focal length equal to the autofocusing distance f_z) after their sizes have been adjusted by lenses L1 and L2 to match the simulation. CAB and CPB are generated by the off-axis hologram method,[14] as depicted in Fig. 1(a2). We used an expanded quasi-plane Gaussian beam modulated by a spatial light modulator (SLM) (L4 and L5 are used to expand the Gaussian beam), and the desired hologram of the CAB/CPB is loaded on the SLM (a hologram is generated by computing the interference between the CAB/CPB wave and a plane wave). Then a $4f$ system (composed of L6 and L7) with a pinhole, which only lets the first order of light modulated by the SLM pass, turns the beam into CAB/CPB. Propagation of the generated SSGB, SEGB, CAB and CPB is monitored by a charge-coupled device and an imaging lens (L8, image beam profiles at different propagation positions). To simulate atmospheric turbulence, we heat an accordion-shaped aluminum foil with an alcohol lamp to generate turbulent air currents in the beam's path.[19] We controlled the turbulence by varying the position of the lamp to adjust the temperature of the hotplate. It is challenging to quantitatively replicate the theoretical turbulence by heating the foil with a lamp; however, the experiment primarily serves as a qualitative confirmation of the conclusions derived from the simulations.

To comprehensively analyze the propagation properties in turbulence, we employed the widely accepted Kolmogorov turbulence theory[27] to calculate the beam propagation. In this case, the index structure parameter C_n^2 is usually used to define the strength of atmospheric turbulence.[28] Then, based on the multiple-phase-screen method,[20,29] we simulated beam propagation in atmospheric turbulence. The modified von Kármán power spectral density (PSD) in Kolmogorov turbulence theory is expressed as[2,28]

$$\phi_n^{mvk}(\kappa)=\frac{0.033C_n^2\exp\left(-\frac{\kappa^2}{\kappa_m^2}\right)}{\left(\kappa^2+\kappa_0^2\right)^{\frac{11}{6}}}, \tag{4}$$

where $\kappa=2\pi\left(f_x\hat{i}+f_y\hat{j}\right)$ is the angular spatial frequency in rad·m^{-1}. The larger κ is, the smaller the PSD $\phi_n^{mvk}(\kappa)$ is, and the influence of turbulence is smaller. $\kappa_m=5.92/l_0$, $\kappa_0=2\pi/L_0$, l_0 is called the inner scale and L_0 is called the outer scale. Finally, under the paraxial condition of Fresnel diffraction, the beam propagation can be simulated via the angular spectrum method.

3. Results and discussion

3.1. Beam propagation in turbulence

Figures 1(b)–1(e) show that SSGB, SEGB, CAB and CPB experience different intensity fluctuations when passing through the same distance with the same magnitude of turbulence. The simulated side-view profiles in Figs. 1(b1)–1(e1) reveal that, compared with the case of no turbulence (see Fig. S1 in the supplementary material), the peak intensities of

the SSGB, SEGB and CAB in turbulence of $C_n^2 = 10^{-8}$ m$^{-2/3}$ are attenuated by 50%, 43% and 41%, respectively, while that of the CPB decreases by only 30%. At the focus, the instantaneous peak intensities of the SSGB and SEGB deviate farther from the original center position than those of the CAB and CPB [Figs. 1(b2)–1(e2) and supplementary visualizations 1–4]. These observations suggest that autofocusing beams exhibit a more robust propagation in turbulence than Gaussian beams, while they maintain autofocusing. These beam features are further corroborated by experiments in atmospheric turbulence. The experimental results match well with the theoretical simulation [insets of Figs. 1(b1)–1(e1) and 1(b3)–1(e3), as well as supplementary visualizations 5–8].

To further support our findings, we dynamically recorded the instantaneous positions of the beams in both simulation and experiment, and their statistical distributions are shown in Figs. 1(b4)–1(e4) and 1(b5)–1(e5). Seemingly, the distribution of autofocusing beams is more concentrated than that of Gaussian beams, evidenced by a smaller centroid deviation. In fact, our calculations reveal that the corresponding statistical positional variances of the SSGB, SEGB, CAB and CPB are 0.0036 mm^2, 0.0041 mm^2, 0.0034 mm^2 and 0.0033 mm^2 in simulation, and 0.0014 mm^2, 0.0022 mm^2, 0.0013 mm^2 and 0.0012 mm^2 in experiment. This clearly indicates that the CPB exhibits the most robust focusing propagation. A similar trend persists even under stronger turbulence conditions such as $C_n^2 = 10^{-7}$ m$^{-2/3}$. For example, the longitudinal focus position of the SSGB and SEGB exhibits significant shifts (from 300 mm to 240 mm and 180 mm) while that of the CAB and CPB remains relatively stable with minor changes (from 300 mm to 264 mm and 270 mm).

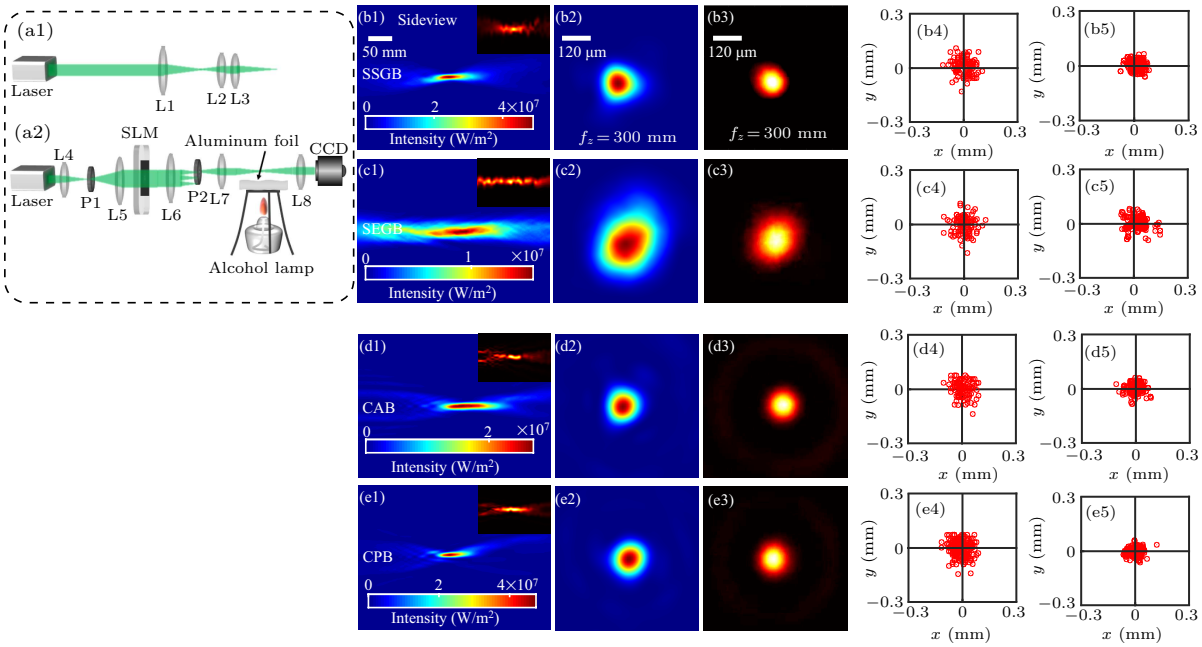


Fig. 1. (a) Schematic diagram of the experimental setups: (a1) for SSGB and SEGB; (a2) for CAB and CPB. L, lens; P, pinhole; SLM, spatial light modulator; CCD, charge-coupled device. (b)–(e) Simulated (Jet) and experimental results (Hot) of the propagation of (b) SSGB, (c) SEGB, (d) CAB and (e) CPB in atmospheric turbulence: (b1)–(e1) side view of propagation; (b2), (b3)–(e2), (e3) intensity distributions at the focus with $z = f_z$ (f_z is the focal length); (b4)–(e4) and (b5)–(e5) the statistical distributions of instantaneous dynamical positions of the beams in (b4)–(e4) simulation and (b5)–(e5) experiment.

3.2. The coherence factor

Light scattering in complex environments causes beam distortion and intensity fluctuation, which leads to decoherence. To assess the impact of turbulence on coherence, we also calculated the modulus of the complex coherence factor (MCF) of the beam.[28,30] See Section 3 in the supplementary material for details.

Figures 2(a)–2(d) depict the variation of the MCF and average intensity distribution for (a) SSGB, (b) SEGB, (c) CAB and (d) CPB at the focus with $C_n^2 = 10^{-9}$ m$^{-2/3}$. In contrast to turbulence-free conditions, all beams demonstrate an amplified average intensity distribution under the influence of turbulence, as depicted in Figs. 2(a2)–2(d2). Furthermore, a comparative examination of the MCFs reveals that the distributions for the CAB and CPB are more extensive than those of Gaussian beams [Figs. 2(a1)–2(d1)]. Since the coherence factor of the beam is also impacted by beam spreading during short-distance propagation,[31] we plotted the change of MCF with respect to $\Delta r/r_0$ ($\Delta r = r - r'$, r_0 is the focus radius) for accessing a more accurate perturbation of turbulence on beam coherence considering C_n^2 values of 10^{-9} m$^{-2/3}$ [Fig. 2(e)], 10^{-8} m$^{-2/3}$ [Fig. 2(f)] and 10^{-7} m$^{-2/3}$ [Fig. 2(g)]. The MCFs

of autofocusing beams consistently outperform those of Gaussian beams, even though all MCFs exhibit rapid decline with escalating turbulence [Figs. 2(e)–2(g)]. In other words, autofocusing beams exhibit more robust propagation.

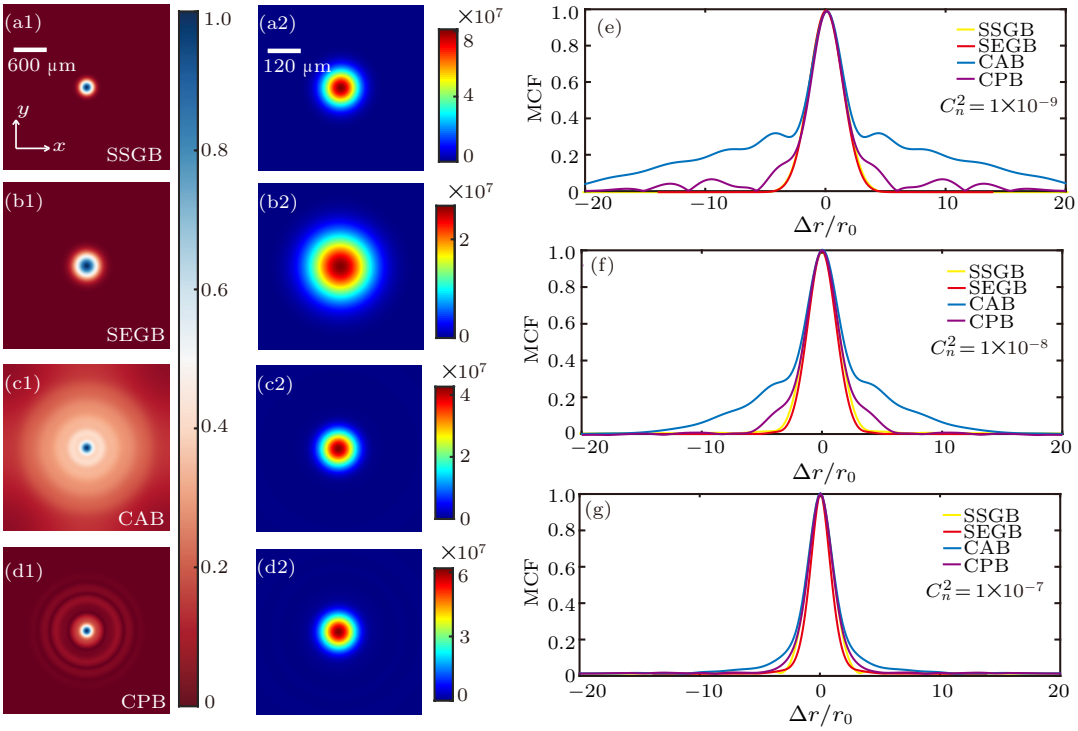


Fig. 2. MCF and average intensity profiles of (a) SSGB, (b) SEGB, (c) CAB and (d) CPB. (a)–(d) Two-dimensional cases for $C_n^2 = 10^{-9}$ m$^{-2/3}$. Panels (e)–(g) show the variations of MCF in one-dimensional form with the ratio of the axial change Δr to the spot radius r_0 in the case of (e) $C_n^2 = 10^{-9}$ m$^{-2/3}$, (f) 10^{-8} m$^{-2/3}$ and (g) 10^{-7} m$^{-2/3}$.

3.3. The scintillation index

Scintillation is the intensity fluctuation caused by random perturbation[32] when a beam passes through turbulence, and is harmful to the beam's propagation. Usually, the scintillation index (SI) is employed to describe such fluctuation, which can be calculated by[2,29]

$$\sigma(r,z)^2 = \frac{\langle I(r,z)^2 \rangle}{\langle I(r,z) \rangle^2} - 1, \tag{5}$$

where σ^2 represents the variance of irradiance, I is the instantaneous intensity and angle brackets stand for the average.

Figures 3(a)–3(d) portray the average intensity fluctuations (SI) of entire beams encompassing SSGBs, SEGBs, CABs and CPBs, considering different structure parameters C_n^2. As expected, there is a noticeable rise in SI as the index structure parameter increases, along with an increase in propagation distance. In this case, the SI in stronger turbulence rises quickly even at smaller distances. Notably, for Gaussian beams, the SI demonstrates a peak at a specific propagation distance, followed by a subsequent decline. This pattern arises due to the autocompensation effect or the diffractive spreading of fragments within the distorted beams, consistent with the report in Refs. [24,33]. Anyway, across all turbulence scenarios, the SI values for SSGBs and SEGBs consistently surpass those for CABs and CPBs in all turbulence cases. This discrepancy highlights the heightened sensitivity of Gaussian beams to intensity fluctuations due to turbulence. This finding reinforces our previous assertion, once again confirming that the propagation of autofocusing beams remains relatively more stable in atmospheric turbulence.

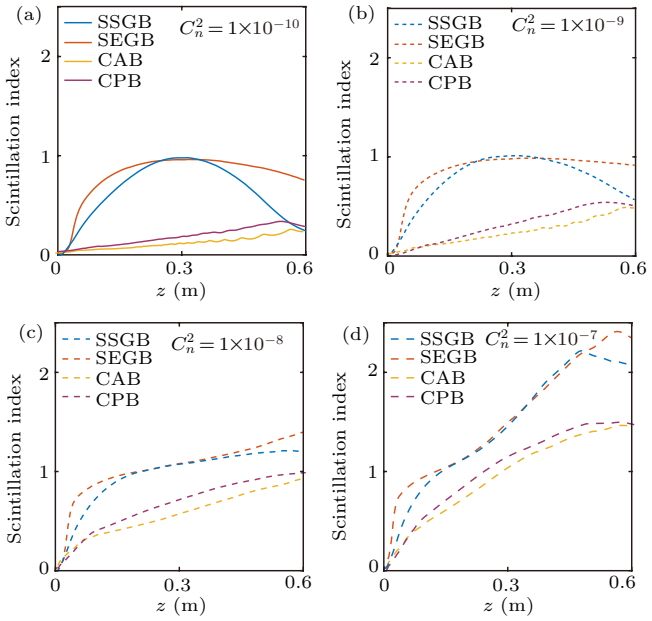


Fig. 3. Scintillation indices of SSGBs, SEGBs, CABs and CPBs vary with the propagation distance z under different index structure parameters C_n^2: (a) 10^{-10} m$^{-2/3}$, (b) 10^{-9} m$^{-2/3}$, (c) 10^{-8} m$^{-2/3}$, (d) 10^{-7} m$^{-2/3}$.

4. Discussion

The results presented above demonstrate that both CABs and CPBs exhibit more robust focusing propagation than Gaussian beams in turbulent environments. This can be explained as follows.

Airy beams and Pearcey beams exhibit a remarkable self-healing property within the field of structured light.[19,23] This intrinsic ability empowers them to rapidly restore their intensity distribution, effectively reverting to a state closely resembling their configuration prior to encountering any obstruction. In more detail, based on catastrophe theory, the acceleration of Airy beams and Pearcey beams originates from the presence of their catastrophic caustics, i.e., fold and cusp caustics. Caustics are regions where the intensity reaches its highest level, and they are closely associated with the existence of stable "singularities".[34,35] Such "singularities" are positions where the second derivative of the full phase of the beam angular spectrum is zero, identified as caustics. Moreover, structural stability is an inherent characteristic of the caustics of Airy and Pearcey beams.[36] In this case, the beams achieve equilibrium, with their inherent characteristics remaining stable against minor disturbances, including subtle phase shifts induced by turbulence. Consequently, these beams exhibit unique attributes such as self-healing properties and a heightened ability to propagate robustly, particularly in turbulent environments. Thus, CABs and CPBs, stemming from Airy beams and Pearcey beams, surpass Gaussian beams in terms of their propagation capabilities within turbulent environments.

Moreover, as presented in Figs. 2(e)–2(g) and 3, in contrast to CPBs, as turbulence intensifies (shifting from $C_n^2 = 10^{-9}$ m$^{-2/3}$ to $C_n^2 = 10^{-7}$ m$^{-2/3}$), CABs exhibit a wider MCF width and smaller SI but change more rapidly. This points to the heightened susceptibility of CABs to the impact of strong turbulence. So, for robust turbulence scenarios, CPB emerges as the superior option for autofocusing propagation due to its stronger autofocusing peak intensity and more stable focus position.

Our results can be extended to other complex environments. For example, when beams pass through a scattering medium of dielectric polystyrene solution, autofocusing beams still show less distortion than Gaussian beams (see Section 5 in the supplementary material). Such a system may further be applied in underwater optical communication and *in vivo* optical trapping.

5. Conclusion

In summary, we have conducted a comprehensive investigation on the propagation behavior of SSGBs, SEGBs, CABs and CPBs in complex environments. Our results indicate that autofocusing beams stand out with superior robust autofocusing performance — showing less intensity distortion and fluctuation than Gaussian beams. Statistical analysis at the focal position supports the heightened stability of autofocusing beams, particularly CPBs. Coherence factor analysis confirms that autofocusing beams exhibit greater coherence than Gaussian beams, reinforcing their superior resistance to turbulence. Examining the variation of scintillation with propagation distance, we find that autofocusing beams experience fewer disruptions and smaller scintillation than Gaussian beams, underscoring the enhanced stability of their intensity. Compared with previous studies, this research presents a more detailed theoretical and experimental comparison of the propagation of autofocusing beams and Gaussian beams in complex environments. These findings hold practical significance, guiding the selection of beams that remain stable, maintain a high focal intensity and propagate effectively in challenging environments. This provides valuable insights for future selection of more stable beam in diverse applications such as optical communication, imaging and optical trapping in complex media.

Acknowledgements

Project supported by the National Natural Science Foundation of China (Grant No. 11604058), Guangxi Natural Science Foundation (Grant Nos. 2020GXNSFAA297041 and 2023JJA110112), Innovation Project of Guangxi Graduate Education (Grant No. YCSW2023083), and Sichuan Science and Technology Program (Grant No. 2023NSFSC0460).

References

[1] Klug A, Peters C and Forbes A 2023 *Adv. Photon.* **5** 016006
[2] Cox M, Mphuthi N, Nape I, Mashaba N, Cheng L and Forbes A 2021 *IEEE J. Sel. Top. Quantum Electron.* **27** 7500521
[3] Bunea A and Gluckstad J 2019 *Laser & Photon. Rev.* **13** 1800227
[4] Ricklin J C and Davidson F M 2002 *J. Opt. Soc. Am. A* **19** 1794
[5] Yang Y J, Ren Y X, Chen M Z, Arita Y and Rosales-Guzmán C 2021 *Adv. Photon.* **3** 034001
[6] Wang Q Y, Fink M and Ma G C 2023 *Phys. Rev. Appl.* **19** 034084
[7] Liu K G, Zhang H K, Du S S, Liu Z Q, Zhang B, Fu X and Liu Q 2022 *Photon. Res.* **10** 2293
[8] Hong P L, Ojambati O S, Lagendijk A, Mosk A P and Vos W L 2018 *Optica* **5** 844
[9] Cao H, Mosk A P and Rotter S 2022 *Nat. Phys.* **18** 994
[10] Bertolotti J and Katz O 2022 *Nat. Phys.* **18** 1008
[11] Efremidis N K and Christodoulides D N 2010 *Opt. Lett.* **35** 4045
[12] Zhang P, Prakash J, Zhang Z, Mills M S, Efremidis N K, Christodoulides D N and Chen Z G 2011 *Opt. Lett.* **36** 2883
[13] Otte E and Denz C 2020 *Appl. Phys. Rev.* **7** 041308
[14] Liang Y, Tan L, Liu N N, Chen K J, Liang H P, Wu H H, Luo B S, Lu F X, Chen H H, Zou B S and Hong P L 2023 *Phys. Rev. Appl.* **19** 014016
[15] Efremidis N K, Chen Z G, Segev M and Christodoulides D N 2019 *Optica* **6** 686
[16] Lu F X, Wu H, Liang Y, Tan L, Tan Z F, Feng X, Hu Y, Xiang Y X, Hu X B, Chen Z G and Xu J J 2021 *Phys. Rev. A* **104** 043524
[17] Moradi H, Jabbarpour M, Abdollahpour D and Hajizadeh F 2022 *Opt. Lett.* **47** 4115
[18] Lu F X, Tan L, Tan Z F, Wu H H and Liang Y 2021 *Phys. Rev. A* **104** 023526

[19] Broky J, Siviloglou G A, Dogariu A and Christodoulides D N 2008 *Opt. Express* **16** 12880

[20] Liang Y, Hu Y, Song D H, Lou C B, Zhang X Z, Chen Z G and Xu J J 2015 *Opt. Lett.* **40** 5686

[21] Ren Y X, Lamstein J, Zhang C S, Conti C, Christodoulides D N and Chen Z G 2023 *Photon. Res.* **11** 1838

[22] Chen X Y, Deng D M, Zhuang J L, Peng X, Li D D, Zhang L P, Zhao F, Yang X B, Liu H Z and Wang G H 2018 *Opt. Lett.* **43** 3626

[23] Ring J D, Lindberg J, Mourka A, Mazilu M, Dholakia K and Dennis M R 2012 *Opt. Express* **20** 18955

[24] Singh S, Mishra S K and Mishra A K 2023 *J. Opt. Soc. Am. B* **40** 2287

[25] Papazoglou D G, Efremidis N K, Christodoulides D N and Tzortzakis S 2011 *Opt. Lett.* **36** 1842

[26] Wang F, Zhao C L, Dong Y, Dong Y M and Cai Y J 2014 *Appl. Phys. B* **117** 905

[27] Jimenez J 2004 *Arbor-Ciencia Pensamiento Y Cul.* **178** 589

[28] Schmidt J 2010 *Numerical Simulation of Optical Wave Propagation With Examples in Matlab* (Washington: Society of Photo-Optical Instrumentation Engineers Press) p. 155

[29] Gu Y and Gbur G 2010 *Opt. Lett.* **35** 3456

[30] Pan Y Q, Zhao M L, Zhang M M, Dou J T, Zhao J, Li B and Hu Y Y 2023 *Opt. & Laser Technol.* **159** 109024

[31] Li C Q, Zhang H Y, Wang T F, Liu L S and Guo J 2013 *Acta Phys. Sin.* **62** 224203 (in Chinese)

[32] Mabena C and Roux F 2019 *Phys. Rev. A* **99** 013828

[33] Berman G P, Gorshkov V N and Torous S V 2011 *J. Phys. B At. Mol. Opt. Phys.* **44** 055402

[34] Hu Y, Bongiovanni D, Chen Z G and Morandotti R 2013 *Phys. Rev. A* **88** 043809

[35] Vaveliuk P, Martinez-Matos O, Ren Y X and Lu R D 2017 *Phys. Rev. A* **95** 063838

[36] Berry M and Upstill C 1980 *IV Catastrophe Optics: Morphologies of Caustics and Their Diffraction Patterns* (Bristol: University of Bristol press) p. 268